Automated Analysis of Collagen Networks via Microscopy

Alejandro Suñe-Auñon, Mario Gonzalez-Arjona, Alejandro Vidal, Javier Lanillos, Arrate Muñoz-Barrutia
Department of Bioengineering and Aerospace Engineering, Universidad Carlos III de Madrid
Instituto de Investigación Sanitaria Gregorio Marañón
Leganés, Spain
mamunoz@ing.uc3m.es

***Abstract*— Full understanding about the interactions between cells and their surrounding environment is needed to characterize the implication of cellular dynamics on physiology and pathology. The knowledge about the composition, the geometry and the mechanical properties of the extracellular matrix is essential for this purpose. In this manuscript, we use an established method for the characterization of 3D collagen networks at fiber resolution in confocal reflection microscopy images. Firstly, a binary mask of the entire network is obtained using steerable filtering and local Otsu thresholding. Secondly, individual collagen fibers are reconstructed by tracking maximum ridges in the Euclidean distance map of the binary mask. The approach was applied to quantify the 3D network geometry of hydrogels polymerized with different collagen concentrations in two *in vitro* platforms: an eight-well culture plate and a microfluidic device. Our results shown similar fiber lengths, fiber persistence lengths and cross-link densities for the fibers of the collagen hydrogels polymerized in different platforms for the same concentration, while the differences on the pore size are large reflecting on the anisotropy of the network polymerized on the microfluidic device.**

Keywords—Collagen networks, confocal reflection microscopy, fiber reconstruction algorithm, microfluidic devices.

I. INTRODUCTION

Extracellular matrix is the three-dimensional environment where cells live. It is mainly composed by collagen [1] and for this reason, collagen-based networks are widely employed as three-dimensional environments to study cell motility and tumor invasion [2]. Moreover, recent works reflect that the composition and mechanical properties of these three-dimensional environments affect cellular phenotypes and migratory patterns [3, 4, 5].

Collagen-I gels belong to a class of materials known as polymers and are modeled as a random network of fibers joint by covalent links. Three-dimensional collagen networks are typically acquired using either confocal reflection microscopy or confocal fluorescence microscopy [6]. The former is the modality chosen to imaging in this work due to its simplicity and lower cost. Namely, fluorescent labeling is avoided together with the associated issues as photobleaching and background noise. However, confocal reflection microscopy suffers from a blind spot [7], leaving the fibers oriented nearly perpendicular to the imaging plane (i.e., cutoff angle) undetected.

Recent works in the literature have been devoted to the quantification of 3D collagen network geometry in confocal microscopy images [8, 9, 10, 11]. Two main steps can be identified in their pipelines: First, a rough binary mask of the network is computed. If a reasonable signal-to-noise ratio through the whole acquired sample is present and the collagen intensity levels in deeper optical sections are homogeneous, intensity-based global thresholding methods are often applied [8, 9]. If the image quality is low, fiber enhancement techniques (such as template-matching [10] or steerable filtering [11]) followed by a local thresholding are used instead. In the second step of the network quantification, the skeleton of the binary mask is computed. For this task, two types of approaches are reported in the literature: simple skeletonization preventing from the identification of the individual fibers [10] and more complex algorithms based on a Euclidean-distance-map-driven skeletonization resulting in the reconstruction of the individual fibers [8, 9, 11].

In this paper, we use the pipeline proposed in [11] to quantify the 3D collagen network geometry at fiber resolution in confocal reflection microscopy images. In the first step, a binary mask of the network is computed using the combination of a steerable filter and a local Otsu threshold. In the second step, a fiber reconstruction algorithm (FIRE) [9] is applied to identify individual collagen fibers. The method is validated on synthetic images generated with the simulator distributed in [9]. An alternative would be to use the validation framework based on a manually generated ground truth proposed in [11]. Our experimental data consist of pure collagen I hydrogels polymerized in a range of concentrations and in two platforms: culture wells and microfluidic devices. Both platforms are well adapted to image acquisition using an inverted microscope. Our experimental results demonstrated that there are differences in the geometry of the hydrogels depending on the platform used for the polymerization that should be taken into account when extracting conclusions from cell migration experiments.

This manuscript is structured as follows: Section II describes the fabrication of the collagen hydrogels and the image acquisition protocol. Section III presents the fiber reconstruction algorithm and the computed measures. In Section IV, the validation of the pipeline using synthetic images and the characterization of the collagen hydrogels when polymerized both in the culture wells and the

ISBN 978-0-9928626-7-1 © EURASIP 2017

microfluidic devices is presented. Finally, in Section IV, some concluding remarks are provided.

TABLE1. Volume (µL) of reagents used for each concentration of hydrogel to obtain a final volume of 400 µL. Note: PBS: Phosphate buffered saline, H_2O: Water, NaOH: Sodium Hydroxide.

Reagent	Collagen Hydrogel Concentration (mg/mL)			
	1,0	*1,5*	*2,0*	*2,5*
Collagen I (3.43 mg/mL)	116,62	174,92	256	291,54
PBS (10x)	40	40	40	40
H_2O	237,38	178,08	94	56,46
NaOH (0.5 N)	6	7	10	12

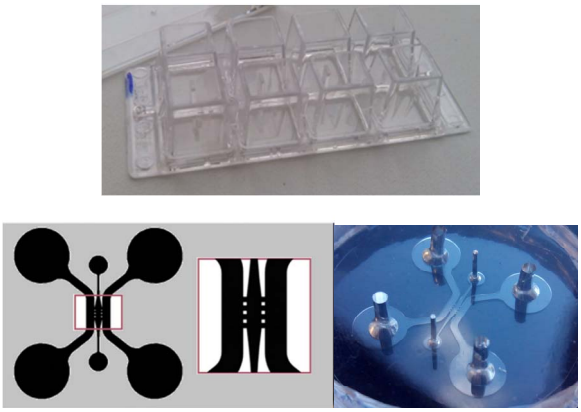

Fig. 1. (Top) Eight-well culture plate; (Bottom, Left) Schema of the microfluidic device. It consists of two lateral channels connected to a central chamber where the hydrogel is loaded; (Bottom, Right) Central chamber and lateral channels in detail.

II. COLLAGEN HYDROGELS

A. Fabrication of hydrogels:

Hydrogels were fabricated by diluting Collagen I from stock (CorningTM, Collagen I, Rat Tail, 3.43 mg/mL) to the desired final concentration using H2O, PBS 10x (adjusted to 1x at the final concentration) and NaOH. The process was performed at 4ºC to prevent early polymerization. Four concentrations of hydrogel were fabricated: 1.0, 1.5, 2.0 and 2.5 mg/mL as described in [8]. First, H2O and PBS were mixed with collagen. Then, NaOH 0.5 N was added to adjust pH to 7-7.5. Microfluidic devices and culture wells were filled with 10 and 300 µL of collagen hydrogel, respectively. The polymerization temperature of 37ºC was kept during 90 min in the case of the microfluidic devices and overnight for the culture wells. After polymerization, collagen fibers were fixed by adding para-formaldehyde 4% (PFA) during 5 min. Table 1 shows the volume of reagents used for each concentration.

B. Polymerization platforms:

1) Culture wells:

Culture wells are chambered coverglass systems made of borosilicate glass (Nunc™ Lab-Tek™). They have eight wells with a working volume of 200-400 µL and a culture area of 0.7 cm2. See Figure 1 for an example. They are sterile and offer an optimized visualization for inverted microscopy.

2) Microfluidic devices:

They were built following the design described in [12]. The device consists of a central chamber (1.44 mm long and 0.68 mm in its widest area) connected to an inlet for hydrogel and cell insertion, and laterally connected to two channels for serum loading. The confinement of the gel was achieved by positioning three pairs of posts along the merging areas of the chamber and the lateral channels (see Figure 1). The devices were loaded using a p20 micropipette with a p200 tip. Devices were made of polydimethylsiloxane (PDMS) by conventional replica-molding processes. The final devices were 40 mm in diameter and 7.5 mm thick.

C. Image acquisition:

Twelve image stacks of each collagen hydrogel concentration were acquired in reflection mode on a Leica SP2 confocal microscope equipped with a glycerol-immersion Plan-Apochromatic 63x (1.3 NA) lens. Each stack is composed by 1024x1024x33 voxels covering a total volume of 238.1x238.1x14.2 μm^3. Illustrative sample crops of the acquired collagen hydrogels images polymerized in the culture wells and the microfluidic devices are shown in Figures 2 and 3, respectively.

III. NETWORK CHARACTERIZATION

To characterize the collagen network geometry of the acquired volumes, we have used an existing pipeline [11]. In this section, we describe its main steps, which are further illustrated in the schematic workflow of Figure 4.

A. Collagen Network Binarization:

The first step to characterize the network geometry is to obtain a precise segmentation of its component fibers. In [11], the input images (see Figure 5 (a)) are pre-processed using a 3D-steerable filter [13]. Its response is computed as the dominant eigenvalue of the Hessian matrix decomposition of a Gaussian filtered version of the input image. The steerable filter acts as an edge detector increasing the contrast of oriented ridges and thus, extending the fibers' signal to noise ratio (see Figure 5 (b)). The fibers are segmented from the steerable filter output computing an Otsu threshold for each z-slice (see Figure 5 (c)) to deal with the fact that the amount of light captured going deeper into the sample is progressively reduced.

B. Fiber Extraction:

The second step of the network characterization approach is the reconstruction of the individual fibers on the collagen network by tracing maximum ridges in the Euclidean distance map on the previously computed binary mask. For this, we rely on the FIRE algorithm [9].

The network is described as $\boldsymbol{N} = \{\boldsymbol{V}, \boldsymbol{X}, \boldsymbol{F}\}$, where $\boldsymbol{V} = [v_1, v_2, \dots, v_N]$ is a list of N numbered vertex or nucleation points, $\boldsymbol{X} = [\boldsymbol{x_1}, \boldsymbol{x_2}, \dots, \boldsymbol{x_N}]$ are the coordinates of the vertexes

ISBN 978-0-9928626-7-1 © EURASIP 2017

($\boldsymbol{x_i} = (x_i, y_i, z_i)$) and $\boldsymbol{F} = [\boldsymbol{f_1}, \boldsymbol{f_2}, \dots, \boldsymbol{f_M}]$ are the M fibers composing the network. Each fiber has associated a list of p vertex points $\boldsymbol{f_i} = [v_{i,1}, v_{i,2}, \dots, v_{i,p}]$ that this fiber passes through.

To discover the network description associated to our collagen hydrogel, first the Euclidean distance map ($\boldsymbol{D}$) corresponding to the binary mask is computed. Then, a set of nucleation points is calculated as follows:

For each grid point $\boldsymbol{x}$, a square box $\boldsymbol{B}$ of radius r and its boundary $\boldsymbol{\partial B}$ is defined as

$$\boldsymbol{B}(\boldsymbol{x}, r) = \{\boldsymbol{y} \in \mathbb{R}^3 | \, \|\boldsymbol{x} - \boldsymbol{y}\|_\infty \leq r\} \quad (1)$$

$$\boldsymbol{\partial B}(\boldsymbol{x}, r) = \{\boldsymbol{y} \in \mathbb{R}^3 | \, \|\boldsymbol{x} - \boldsymbol{y}\|_\infty = r\}, \quad (2)$$

The nucleation points ($\boldsymbol{V}$) are defined as the local maxima inside each box

$$\boldsymbol{V} = \{\boldsymbol{x} \in \mathbb{R}^3 | \, \boldsymbol{D}(\boldsymbol{x}) \geq \boldsymbol{D}(\boldsymbol{y}), \forall \boldsymbol{y} \in \boldsymbol{B}(\boldsymbol{x}, r)\} \quad (3)$$

After that, every nucleation point in $\boldsymbol{x} \in \boldsymbol{V}$ is extended into a short fiber segments following the direction given by the local maxima of $\boldsymbol{D}$ in $\boldsymbol{\partial B}(\boldsymbol{x}, \boldsymbol{D}(\boldsymbol{x}))$, which are separated from $\boldsymbol{x}$ at least $\theta_{LMPdist}$ grid points. Next, the short segments with similar orientation in the corresponding tips, closer than θ_{linkd}, are iteratively linked into longer fiber segments. Finally, the segments shorter than θ_{dang-L} are removed. The rest are established as individual collagen fibers forming the network (see Figure 5 (d)).

Once the individual collagen fibers have been reconstructed, four geometric network parameters are estimated, namely, the fiber length, the fiber persistence length, the crosslink density and the pore size. The fiber length is computed by aggregating Euclidean distances between successive pairs of fiber points. The persistence length is a measure of the stiffness of the collagen hydrogel. Namely, the pieces of a polymer that are shorter than the persistence length are mechanically flexible. This parameter is calculated for each fiber by finding the best least squares fitting exponential for the cosines of the angle difference between the contiguous vertexes [9]. A cross-link is formally defined as a bound that links one polymer chain to another. In our case, we consider that two chains are cross-linked when the distance between them is below the voxel size. The cross-link density is defined as the number of crosslink points per the total fiber length of the network. Finally, the size of the pores is defined as the average radius of the spheres filling the fluid phase spaces [8].

IV. EXPERIMENTAL RESULTS

Synthetic and real datasets were analyzed in a desktop computer equipped with an Intel-Core i7-4770 3.4 GHz processor and 16 gigabytes of RAM.

A. Synthetic generated volumes:

The simulator given as part of the fiber extraction package [9] was used to create three dimensional artificial collagen network's images, so as to test the performance of the algorithm.

Twelve synthetic volumes were created simulating the collagen gel concentrations [1, 1.5, 2, 2.5 mg/mL] given

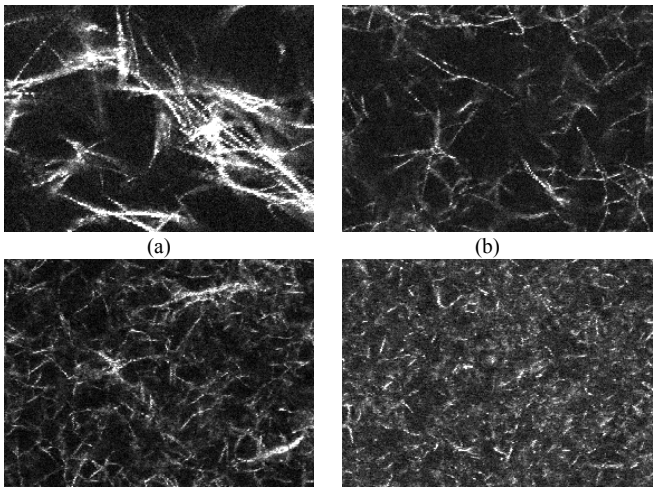

Fig. 2. Sample middle z-slice crops of size $64.64\mu m \times 47.43\mu m$ from the confocal reflection microscopy images of the collagen hydrogel volumes polymerized on a well culture plate. Concentration (mg/mL): (a) 1.0, (b) 1.5, (c) 2.0, and (d) 2.5.

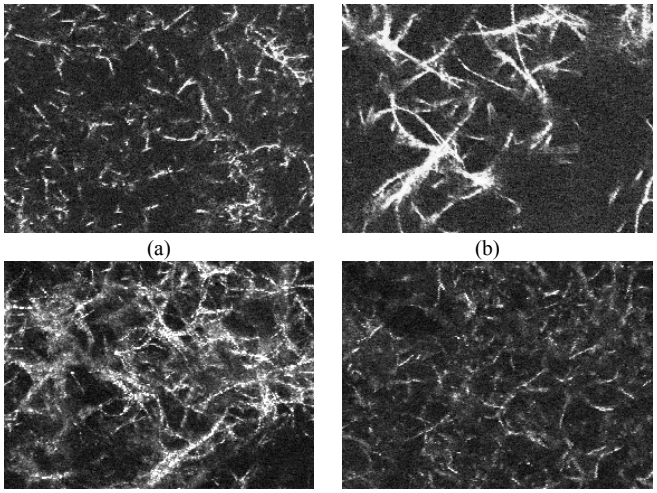

Fig. 3. Sample middle z-slice crops of size $64.64\mu m \times 47.43\mu m$ from the confocal reflection microscopy images of the collagen hydrogel volumes polymerized on a microfluidic device. Concentration (mg/mL): (a) 1.0, (b) 1.5, (c) 2.0, and (d) 2.5.

standard values for the volume size, voxel size, fiber diameter and fiber length distribution. The synthetic volumes were processed using our pipeline. The difference between the cumulative distribution function of fiber length and fiber persistence length's distribution between the synthetic images and the results obtained from the output of the FIRE pipeline was computed (data not shown). A certain mismatch was observed for all concentrations possibly caused by the short fibers in the synthetic images being removed by the FIRE post-processing steps. Estimated pore sizes were also compared (data not shown) giving small differences (below 6%) for all the concentrations.

B. Collagen hydrogel volumes:

The processing pipeline was applied to the whole dataset (see Section 2). The median values of the four parameters we

ISBN 978-0-9928626-7-1 © EURASIP 2017

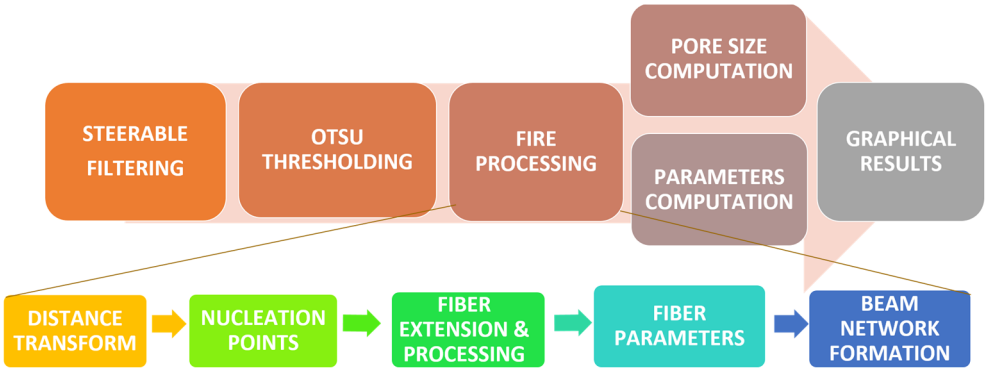

Fig. 4. Schematic workflow of the pipeline. The output of the Otsu thresholding is the binarized collagen network. The main steps of the FIRE algorithm are summarized in the second row. The output of the FIRE processing gives the individual fiber reconstructions, which are used to compute the parameters that characterize the network geometry including the pore size. In a final step, the results are graphically displayed.

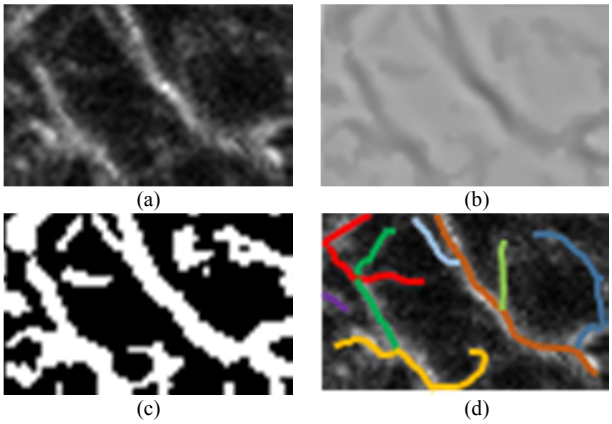

Fig. 5. Illustration of the main steps of the algorithm. (a) A middle z-slice crop from an image of a collagen hydrogel with 1 mg/mL concentration. (b) The response of the steerable filter. In this case, the fibers correspond to a negative response (i.e., dark values). (c) The binary mask corresponding to the sample collagen hydrogel network. (d) The reconstruction of individual fibers where each individual fiber has been labeled with a different color.

compute to characterize the network geometry: fiber length, fiber persistence length, cross-link density and pore size, per collagen hydrogel concentration are presented in Tables 2 (culture wells) and 3 (microfluidic devices).

For both platforms, fiber length increases with the concentration to reach saturation at 2 mg/mL. There are not significant differences between platforms ($p>0.05$, Wilcoxon text), but a slight increment for culture wells is observed.

Fiber persistence length distribution, as expected, is similar for all concentrations. This parameter is set by the nature of the collagen proteins and it should not change in value neither with differences in concentration nor depending on the polymerization platform. There are not significant differences between platforms ($p>0.05$, Wilcoxon test).

In terms of the pore size, in both platforms, we observe that this parameter decreases as the collagen hydrogel increases. Moreover, the pore size of the collagen hydrogels polymerized in the microfluidic device is significantly larger ($p<0.05$, Wilcoxon test) than when they polymerized in the culture wells. In our view, this result may be due to the laminar flow that is created when the un-polymerized hydrogel is loaded into the microfluidic device and the anisotropic nature of the polymerization happening in the device (i.e., mostly unidirectional fiber polymerization). It could also be partly caused by human error consequence of manually loading the devices.

Finally, the crosslink density keeps mostly constant for both platforms independently of the collagen concentration. There are not significant differences between platforms ($p>0.05$, Wilcoxon text).

V. Discussion and Conclusions

In this manuscript, we have exploited the reliable and robust pipeline presented in [11] to give an initial, distinctive characterization of collagen hydrogels polymerized at different concentrations in both culture wells and microfluidic devices. This characterization constitutes the basis on which to build in further studies about how collagen disposition and geometry influences cell-matrix interactions and determines cellular migratory patterns.

Previous efforts to characterize collagen networks were performed on hydrogels polymerized in culture wells. Nowadays, there are increasingly more studies performed in microfluidic devices. In this work, we have given preliminary results demonstrating the importance of characterizing the networks on the platforms in which the actual experiments are performed because a significant variation of the network parameters can be caused by the geometry of the device and the loading conditions.

As commented previously, confocal reflection microscopy has a limitation. It suffers from a blind spot [7]. Namely, the

ISBN 978-0-9928626-7-1 © EURASIP 2017

emission from fibers with orientation exceeding a cutoff angle from the imaging plane goes entirely undetected. The blind spot affecting the confocal reflection microscopy images introduces an error in the estimation of the pore size. However, if the cutoff angle for the missing fibers is known, it is possible to compute a correction as was done in [6] for collagen hydrogels polymerized in culture wells. Currently, we are implementing this correction for the estimation of the pore size in both platforms.

Although our results are quite satisfactory, the iterative fiber reconstruction process implies a high computational demand. It could be worthy to explore alternative approaches to reduce the load as the one proposed in [14] that uses Stretching Open Active Contours to extract actin network centerlines. Even further, when the study of matrix remodeling using time-lapse experiments is the objective, using fiducial markers (i.e., fluorescent nanobeads) as subrogates of the collagen fibers [15] or graph theory to compute metrics characterizing the hydrogel geometry [16] should be explored.

TABLE 2. The median values of fiber length, fiber persistence length, network pore size and crosslink density per collagen hydrogel concentration when polymerized in a well culture plate. All the measures are in µm, except the crosslink density (crosslinks/µm).

Measures	**Collagen Hydrogel Concentration (mg/mL)**			
	1,0	***1,5***	***2,0***	***2,5***
Fiber length	5.22	5.89	6.66	6.82
Fiber pers. length	3.91	4.05	4.12	4.14
Pore size	2.96	1.88	1.42	1.31
Crosslink dens.	0.26	0.25	0.23	0.22

TABLE 3. The median values of fiber length, fiber persistence length, network pore size and crosslink density per collagen hydrogel concentration when polymerized in a microfluidic microdevice. All the measures are in µm, except the crosslink density (crosslinks/µm).

Measures	**Collagen Hydrogel Concentration (mg/mL)**			
	1,0	***1,5***	***2,0***	***2,5***
Fiber length	4.89	5.03	5.91	5.90
Fiber pers. length	3.98	3.50	3.98	4.12
Pore size	5.12	4.42	2.52	1.75
Crosslink dens.	0.25	0.27	0.25	0.25

ACKNOWLEDGMENT

This work was partially supported by the Spanish Ministry of Economy and Competitiveness (TEC2013-48552-C2-1-R, TEC2015-73064-EXP and TEC2016-78052-R) and FEDER funds through 'Programa Operativo de Empleo Juvenil y la Iniciativa de Empleo Juvenil (YEI)' from Madrid Local Government.

REFERENCES

[1] K. Gelse, E. Poschl, and T. Aigner, "Collagens—structure, function, and biosynthesis", Advanced Drug Delivery Reviews, vol. 55, no. 12, pp. 1531-1546, 2003.

[2] J. A. Pedersen, and M. A. Swartz, "Mechanobiology in the third dimension", Annals of Biomedical Engineering, vol. 33, no. 11, pp. 1469-1490, 2005.

[3] J. Brabek, C. T. Mierke, D. Rosel, P. Vesely, and B. Fabry, "The role of the tissue microenvironment in the regulation of cancer cell motility and invasion", Cell Communication and Signaling, vol. 8, no. 1, pp. 22, 2010.

[4] S. I. Fraley, P. H. Wu, L. He, Y. Feng, R. Krisnamurthy, G. D. Longmore, and D. Wirtz, "Three-dimensional matrix fiber alignment modulates cell migration and MT1-MMP utility by spatially and temporally directing protrusions", Scientific Reports, vol. 5, pp. 14580-14580, 2014.

[5] M. Anguiano, C. Castilla, M. Maska, C. Ederra, R. Pelaez, X. Morales, *et al*., "Characterization of three-dimensional cancer cell migration in mixded collagen-matrigel scaffolds using microfluidics and image analysys," PloS One, vol. 12, no. 2, pp. e0171417, 2017.

[6] N. R. Lang, S. Munster, C. Metzner, P. Krauss, S. Schurmann, J. Lange, *et al*., "Estimating the 3D pore size distribution of biopolymer networks from directionally biased data", Biophysical Journal, vol. 105, no. 9, pp. 1967-1975, 2013.

[7] L. M. Jawerth, S. Munster, D. A. Vader, B. Fabry, D. A. Weitz, "A blind spot in confocal reflection microscopy: The dependence of fiber brightness on fiber orientation in imaging biopolymer networks", Biophysical Journal, vol. 98, no. 3, pp. L1-L3, 2010.

[8] W. Mickel, S. Munster, L. M. Jawerth, D. A. Vader, D. A., Weitz, A. P. Sheppard, *et al*., "Robust pore size analysis of filamentous networks from three-dimensional confocal microscopy", Biophysical Journal, vol. 95, no. 12, pp. 6072-6080, 2008.

[9] A. M. Stein, D. A. Vader, L. M. Jawerth, D. A. Weitz, and L. M. Sander, "An algorithm for extracting the network geometry of three-dimensional collagen gels", Journal of Microscopy, vol. 232, no. 3, pp. 463-475, 2008.

[10] P. Krauss, C. Metzner, J. Lange, N. Lang, and B. Fabry, "Parameter-free binarization and skeletonization of fiber networks from confocal image stacks," PLoS ONE, vol. 7, no. 5, pp. 463-475, 2008.

[11] M. Maska, C. Ederra, J. Fernandez-Marques, A. Munoz-Barrutia, M. Kozubek, and C. Ortiz-de-Solórzano, "Quantification of the 3D collagen network geometry in confocal reflection microscopy", Proceedings of the 2015 IEEE International Conference on Image Processing (ICIP'15), pp. 1791-1794, 2015.

[12] Y. Shin, S. Han, J. S. Jeon, K. Yamamoto, I. K. Zervantonakis, R. Sudo, *et al*., "Microfluidic assay for simultaneous culture of multiple cell types on surfaces or within hydrogels", Nature Protocols, vol. 7, no. 7, pp. 1247-1259, 2012.

[13] M. Jacob, and M. Unser, "Design of steerable filters for feature detection using canny-like criteria", IEEE Transactions on Pattern Analysis and Machine Intelligence, vol. 26, no. 8, pp. 1007-1019, 2004.

[14] T. Xu, D. Vavylonis, and X. Huang, "3D actin network centerline extraction with multiple active contours," Medical Image Analysis, vol. 18, pp. 272-284, 2014.

[15] R. J. Bloom, J. P. George, A. Celedon, S. X. Sun, and D. Wirtz, "Mapping local matrix remodeling induced by a migrating tumor cell using three-dimensional multiple-particle tracking," Biophysical Journal, vol. 95, pp. 4077-4088, 2008.

[16] C. C. Bilgin, A. W. Lund, A. Can, G. E. Plopper, and B. Yener, "Quantification of three-dimensional cell-mediated collagen remodeling using graph theory, ", PLoS ONE, vol. 5, no. 9, pp. e12783, 2010.